Construction and Building Materials 427 (2024) 136011

Contents lists available at ScienceDirect

Construction and Building Materials

journal homepage: www.elsevier.com/locate/conbuildmat

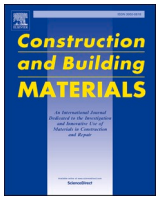

Evaluation of MSW incineration bottom ash for environmentally safe geotechnical applications

B.S. Bandarra [a,*], L. Monteiro [b], G. Veloso [b], P. Abreu [a], H. Sousa [b], R.C. Martins [a], J.L. Pereira [c], P. A.L.F. Coelho [b], M.J. Quina [a]

[a] University of Coimbra, CERES, Department of Chemical Engineering, 3030-790 Coimbra, Portugal
[b] University of Coimbra, CITTA, Department of Civil Engineering, 3030-788 Coimbra, Portugal
[c] CESAM – Centre for Environmental and Marine Studies, Department of Biology, University of Aveiro, 3810-193 Aveiro, Portugal

ARTICLE INFO

Keywords:
IBA
Chemical analysis
Ecotoxicity
Mechanical properties
Geotechnical applications
Circular economy

ABSTRACT

Circular economy envisages resource efficiency and minimization of the negative impacts of waste on the environment and human health. This work considers municipal solid waste incineration bottom ash (IBA) for safe use in geotechnical works, through physical, chemical, ecotoxicological, and geotechnical analysis of samples with different weathering periods. Low leaching potential and no relevant ecotoxic effects were found for IBA. Better compaction was obtained for IBA mixtures with sand. All materials showed reasonable permeability after compaction. IBA stiffness and shear strength values, consistently assessed through different tests, were within dense granular soils range. Weathering seems to positively influence IBA geotechnical properties, which in any case seem compatible with environmentally safe and sustainable geotechnical applications.

1. Introduction

World production of municipal solid waste (MSW) keeps increasing due to the present production and consumption patterns, which should reach 3.4 billion tonnes by 2050 [1]. The same trend has been observed in the European Union (EU), where around 237 million tonnes of MSW (EU-27) were generated in 2021 [2]. This has been one of the main challenges for urban sustainable development, and incineration in Waste-to-Energy (WtE) plants has been one of the main management strategies adopted by developed countries to deal with it. In the EU, around 27% of MSW are incinerated [3]. Incineration plays a key role in the treatment of unsorted waste and residual streams from recycling activities, reducing waste volume by about 90%, producing energy, and eliminating potentially unsafe materials/molecules and pathogens [4,5]. The main solid residue from this process is incineration bottom ash (IBA), accounting for 20–25% of MSW incinerated [6]. IBA is a very heterogeneous material with a wide particle size distribution mainly composed of minerals, ceramics, metallic compounds, and glass [7]. It is relevant to prioritise the valorisation of IBA over landfilling given the high produced amount, promising properties, and the need to avoid landfilling as highlighted by the waste management hierarchy established in the EU waste framework directive (WFD; Directive 2008/98/EC). The metallic fraction is generally recovered to be applied in the metal industry, while the mineral fraction has been managed through diverse strategies [8–10]. In the EU, the mineral fraction is not valorised in certain Member States, while in others different applications are permitted but the requirements for chemical analysis prior to application are diverse [9]. In fact, IBA potential to cause negative environmental impacts has been a central topic in this regard. IBA may contain potentially toxic metals (PTM) and soluble salts with environmental hazard potential, usually more concentrated in the finest fraction [11–14]. Different pre-treatments may be applied to reduce this potential, and natural weathering is the most common one. Natural weathering results in a more stable material through its storage outdoors for 6–20 weeks and the consequent neoformation and hydration of mineral phases through carbonation and oxidation reactions, resulting in a pH decrease from 10–13 to 8–10 and the encapsulation of some PTM [8,10,14–18].

IBA is usually classified as non-hazardous [19,20] but it is a mirror entry in the European List of Waste (LoW; Decision 2014/955/EU), meaning it may be classified as hazardous (19 01 11*) or non-hazardous (19 01 12) as a function of the assessment outcome of waste hazard properties defined in Commission Regulation (EU) 1357/2014, and persistent organic pollutants (POP) content (Regulation (EU)

* Corresponding author.
E-mail address: bsbandarra@eq.uc.pt (B.S. Bandarra).

https://doi.org/10.1016/j.conbuildmat.2024.136011
Received 21 February 2024; Accepted 25 March 2024
Available online 15 April 2024

2019/1021). The Hazard Property HP 14 ("ecotoxic") is related to potential environmental impacts and the methods for its determination are not consensual. The value of ecotoxicological tests has been increasingly recognized for the assessment of complex matrixes (such as various types of waste) since they account for the effects of all constituents, their interactions, and bioavailability, thus more realistically evaluating waste environmental impacts [21–23]. Some studies evaluated IBA with a range of test organisms and endpoints, with varying outcomes [24–29].

Applications that have been considered for IBA include artificial aggregates or mineral addition in civil engineering applications such as road constructions (base, subbase, embankments, asphalt concretes), cement and concrete production, ceramics manufacture, as well as use in noise barriers, pipe bedding, recovery in landfills, and filling and restoration of degradable areas from extractive activities [4,8,9,11,17,30]. Nonetheless, its use as a secondary aggregate in road construction is one of its main potential applications [8–10,31]. However, important geotechnical properties (such as compaction, compressibility, and shear strength) of IBA and its mixtures with natural aggregates are not comprehensively evaluated in the literature, and few studies can be found with this information, particularly for the EU [29,32–40]. Moreover, IBA presents variable mechanical properties, which may prevent extensive use [4,41]. Therefore, alongside environmental assessment, the technical performance of IBA should be evaluated considering the aimed application.

The development of waste legislation and policies to promote sustainable waste management has been one of the main targets of the EU. In this context, the EU circular economy policy [42] aims at using wastes as resources in suitable applications, hence promoting efficient use of resources and landfilling reduction. The use of secondary raw materials contributes to reducing natural resource depletion and the consequent impact of resource mining. Landfills require land space and high costs to maintain engineered sanitary conditions, favour the loss of valuable resources, and entail secondary pollution possibilities (e.g., groundwater pollution and release of gases such as methane, a greenhouse gas) [19]. It is important to pursue the utilization of secondary materials due to the high demand for construction materials, the finite nature of natural resources, and issues related to landfilling. Geotechnical applications seem a relevant approach for IBA use given volume requirements, allowing to save raw materials and the desirable use of IBA as much as possible. The present study is part of a wider investigation that focused on the assessment of weathered IBA for environmentally safe geotechnical applications. Previous research aimed at evaluating the basic physical and mechanical properties of IBA alone and in a mixture with quartz sand (30% IBA:70% sand) from a geotechnical perspective, simultaneously analysing the chemical characteristics of these materials and the suitability of a battery of biotests for HP 14 assessment [29]. This work aims at evaluating weathered IBA in compacted conditions regarding technical performance and environmental impacts targeting environmentally safe geotechnical applications within the circular economy framework, namely those involving heavy compaction in the field, such as road and railway bases, subbases, subgrades, and embankments. Geotechnical properties, including advanced mechanical testing to evaluate the strength and stiffness of the tested materials, were assessed in IBA 3-months aged (IBA-3M) and 1-year aged (IBA-12M) to analyse if differences would arise for different periods of weathering. Moreover, two different mixtures (M1 and M2) of IBA 3-months aged with quartz sand were evaluated for analysing the influence of sand addition in geotechnical properties: M1 – 90% IBA:10% sand; M2 – 60% IBA:40% sand. According to our knowledge, this work is the first to encompass a multidisciplinary and comprehensive assessment of compacted IBA including chemical, ecotoxicological, and geotechnical evaluations as well as the assessment of the influence of factors such as aging and different mixtures with sand, aiming at promoting real-world efficient and sustainable engineering applications.

2. Materials and methods

2.1. Materials

Two IBA samples were provided by a European WtE plant which works with mass-burning technology. One sample was subjected to outdoor weathering/ageing for 3 months (IBA-3M) and the other was aged for ca. 1 year (IBA-12M). Ferrous metals were previously removed in the WtE plant through magnetic separation. The received samples were dried at room temperature and stored for further use. All tests were carried out with diameter of particles (dp) <9.5 mm, except shear box and oedometer tests which were performed with dp<2 mm due to equipment size specifications. Representative subsamples were obtained through a sample splitter. Whenever needed, subsamples were crushed by a ball mill. IBA eluates were obtained for chemical and ecotoxicological testing following EN 12457–2 (liquid/solid - L/S - ratio of 10 L/kg for 24 h with distilled water; filtration through 0.45 μm pore membrane). The fraction with 4<dp<9.5 mm was milled and mixed with the fraction with dp<4 for leaching procedures. Furthermore, quartz sand from Leiria (Portugal) was used to prepare mixtures with the 3-months aged IBA with IBA:sand ratios of 90%:10% (M1) and 60%:40% (M2) for geotechnical evaluation. Sand was also sieved to dp<2 mm to perform shear box and oedometer tests with the mixtures.

2.2. Analysis of potential environmental impact

2.2.1. Chemical parameters

Moisture and volatile solids (estimation of organic matter, OM) were determined at 105 °C for 24 h and 550 °C for 2 h, respectively, based on EPA Method 1684. Electrical conductivity (EC) and pH were measured in IBA eluate with a Consort C1020 multiparameter analyser. The elemental composition of solid IBA (after acid digestion) and concentrations in its eluate was analysed through flame atomic absorption spectroscopy (FAAS) and inductively coupled plasma mass spectrometry (ICP-MS). FAAS was carried out using Analytikjena ContrAA 300 equipment and Aspect CS 2.1.1.0 Tech:Flame software. Previously, microwave assisted acid digestion of milled IBA (dp<0.075 mm) was conducted with a TRANSFORM 680 Microwave Digestion System (Aurora Instruments) following EPA Method 3051 A. ICP-MS analysis was performed using Thermo Elemental X-series spectrometer in a certified laboratory. Quality control was safeguarded by the analysis of certified reference materials, blanks, and testing samples in triplicate. Chlorides and sulphates were measured in IBA eluates by ion chromatography with Dionex ICS 5000+ equipment.

2.2.2. Ecotoxicological tests

Different concentrations of initial IBA eluates (100%) were prepared with distilled water for ecotoxicological assessment, all being analysed with their natural pH. All organisms were tested with eluate concentrations of 3.125, 6.25, 12.5, 25, 50, and 100%(v/v), except *A. fischeri* for which the 3.125% concentration was not tested. For this purpose, a biotest battery covering species from different trophic/functional levels previously evaluated [29] was used. Tests were performed based on standard methods (Table 1), which are further detailed by the authors elsewhere [43,44]. Median effect concentrations (EC_{50}) were considered as ecotoxicological references a priori. Significant effects of eluates were analysed using one-way ANOVA ($p<0.05$), followed by the Dunnett's test ($p<0.05$) to identify treatments leading to significant effects on test organisms. The nonparametric Kruskal-Wallis H test was used whenever the normality or homoscedasticity assumptions of the parametric approach were not met (Kolmogorov-Smirnov test and Levene's test, respectively; $p<0.05$).

Table 1
Biotest battery and methods followed.

Test organism	Endpoint (%)	Duration	Temperature (°C)	Light	Standard
Aliivibrio fischeri	Luminescence inhibition	30 min	15 ± 1	-	ISO 11348–2 [45]
Raphidocelis subcapitata	Growth rate inhibition	96 h	23 ± 1	Continuous	OECD guideline 201 [46] adapted to 24-well microplates [47]
Lemna minor	Growth rate inhibition considering frond number and dry weight	7 d	23 ± 1	Continuous	OECD guideline 221 [48] adapted to 6-well microplates [49]
Daphnia magna	Immobilisation	48 h	20 ± 2	16 h^L:8 h^D	OECD guideline 202 [50]
Lepidium sativum	Seed germination and root growth inhibitions	72 h	25 ± 1	-	ISO 18763 [51]

2.3. Geotechnical evaluation

2.3.1. Physical properties

The initial particle size distributions of test materials were obtained by dry sieving (dp≥2 mm), wet sieving (0.075≤dp<2 mm), and sedimentation (dp<0.075 mm). The granulometric curve of mixtures was determined as the weighted average of measurements for sand and IBA. D_{60}, D_{30}, and D_{10} represent, respectively, the grain size diameters below which 60, 30, and 10% of particles, in weight, are finer and were determined based on the granulometric curve. Coefficients of uniformity (C_U) and curvature (C_C) were calculated as $C_U = D_{60}/D_{10}$ and $C_C = D_{30}^2/(D_{10}\times D_{60})$, respectively. The density of solid particles (G) of quartz sand and IBA was obtained through pycnometry following ASTM D854–14. Regarding IBA, G was first determined for three different size fractions (dp<0.425 mm; 0.425<dp<2 mm; 2<dp<9.5 mm) to evaluate the potential effects of particles different composition. The G of mixtures was calculated as the weighted average of values determined for sand and IBA. The liquid limit (LL) was determined through the cone penetrometer method based on BS 1377–2:1990 (dp<0.425 mm). This method allows to evaluate low plasticity materials more easily than the commonly used Casagrande apparatus, while providing more reproducible results since it depends less on the operator judgement. The plastic limit (PL) was obtained based on ASTM D4318–17e1 (dp<0.425 mm) using the hand-rolling method, i.e., by rolling spheres against a glass plate to gradually reduce water content until the cylindrical filament with about 3 mm diameter crumbled. The plasticity index (PI) was calculated as the difference between LL and PL.

2.3.2. Compaction

The modified Proctor test was conducted to determine the optimum water content (w_{opt}) and the maximum dry unit weight (γ_{dmax}) in compaction of tested samples based on ASTM D1557–12(2021). Taking into account IBA particles size and the compaction means commonly used in the field for embankments construction, a small mould and heavy compaction energy were selected. The Proctor test was not performed with mixture M1 since it was considered that the low percentage of sand would not significantly alter the w_{opt} and the γ_{dmax} of IBA-3M. Thus, the values obtained for IBA-3M were considered for the compaction of M1 whenever needed. Six subsamples of about 2 kg of each sample were dried at 40 °C for 48 h. Water percentages of 12%, 14%, 16%, 18%, 20%, and 22% were added to IBA samples, and 8%, 10%, 12%, 14%, 16%, and 18% to M2. Each subsample was then divided into five equal fractions, each being placed in the mould and subjected to 25 falls of a heavy compaction hammer (4.54 kg) falling from a 457 mm height. For each subsample, 3 replicates were weighed before and after drying at 105 °C for 24 h to measure the water content, w (%) (Eq. 1). The dry unit weight, γ_d (kN/m^3), was calculated for each subsample through Eq. 2, and compared to the saturation curves (Eq. 3). The w_{opt} and the γ_{dmax} for compaction were obtained from the peak of the plotted graph. Saturation curves indicate voids percentage or the degree of saturation at different points of compaction curves and were plotted using the average G for each material.

$$w = \frac{\text{Water weight}}{\text{Dry soil weight}} \times 100 \quad (1)$$

$$\gamma_d = \frac{\gamma}{1+w} \quad (2)$$

$$\gamma_d = \frac{G \times \gamma_w}{1 + (w \times G/S)} \quad (3)$$

Where: $\gamma = P/V$ - unit weight (kN/m^3); P – total weight of the sample (kN); V – total volume of the sample (m^3); G - solid particles density, γ_w – unit weight of water (kN/m^3); S –saturation degree.

2.3.3. One-dimensional compressibility

All samples were evaluated regarding one-dimensional compressibility through oedometer tests based on ASTM D2435–04. All specimens were prepared by compaction, aiming at replicating the modified Proctor test. Thus, the w_{opt} previously obtained with Proctor was used. Compaction was performed in the Proctor mould containing the rigid ring of the oedometer, three layers of material being compacted with an energy per layer similar to that used in Proctor. In the oedometer ring, samples were subjected to cycles of vertical loading and unloading resulting in the following vertical effective stresses (σ'_v): 1.4, 8.5, 16, 30, 58, 114, 227, 452, 1016, 227, 58, 16, 58, 227, 1016, 2143, 4398, 1016, 227, 58, 8.5, and 1.4 kPa. Load changes followed stabilization of settlements. Each sample was submerged after σ'_v=58 kPa, with no load changes occurring for 24 h, to assess the collapse or expansion potential of these materials due to saturation. Saturation was maintained for the subsequent loading and unloading stages. The vertical displacement (mm) over time for each applied stress was measured by Linear Variable Differential Transformer (LVDT) transducers connected to oedometers. The void ratio (e) per applied vertical effective stress (σ'_v) was obtained from Eqs. 4–5. As previously mentioned (Section 2.1), this test was performed with dp<2 mm. Regarding IBA-12M, the average G for dp<2 mm was used for calculations given the material heterogeneity, while the total average G was used for IBA-3M.

$$e_0 = \frac{G \times \gamma_w}{\gamma_d} - 1 \quad (4)$$

$$e = e_0 + \frac{\Delta h \times (1+e_0)}{h_0} \quad (5)$$

Where: γ_d – dry unit weight (kN/m^3); e_0 – initial void ratio; G – solid particles density; γ_w – unit weight of water (= 9.81 kN/m^3); Δh – samples height variation in the oedometer ring (mm); h_0 – samples initial height in the ring (mm).

The compression (C_c) and recompression indexes (C_r) were determined as the slope of the virgin and recompression lines, respectively, from the e-logσ'_v plots. The coefficient of consolidation (C_v) was determined using Taylor's method (Eq. 6). In this method, height variation is plotted as a function of the square root of time regarding a single loading/unloading to obtain the time corresponding to a consolidation of 90% (t_{90}). The coefficient of permeability (k) was estimated through Eq. 7.

$$C_v = \frac{0.848 \times d^2}{t_{90}} \quad (6)$$

$$k = C_v \times \gamma_w \times m_v \quad (7)$$

Where: d – drainage path (in the oedometer test, equal to half of the sample height); t_{90} - time corresponding to a degree of consolidation of 90%; m_v – coefficient of volume compressibility.

2.3.4. Shear strength: shear box tests

All samples were analysed regarding shear strength under different vertical (normal) effective stresses ($\sigma'_v = \sigma'_n$) using the shear box test, which is commonly applied in road and backfill engineering for a quick shear strength assessment given its convenience and effectiveness [35]. Samples were also compacted to replicate the Proctor test, three layers of material being compacted by the Proctor hammer directly in the shear box with the w_{opt} obtained from Proctor test. Each layer boundaries were at least 4 mm distant from the middle division of the shear box to avoid influencing the shear plane. The hammer fell on an iron cube instead of directly on samples given the geometry of the shear box, and 33 falls were applied on each layer to replicate the specific energy from the Proctor test. The shear box dimensions were 10 cm×10 cm x 3.7 cm. Three tests were conducted on each material with σ'_v (=σ'_n) of 50, 100, and 200 kPa. Samples were sheared at constant speed of ≈ 0.6 mm/min, which were assumed to be low enough to consider the test drained. Nevertheless, the test was repeated for σ'_v=100 kPa using a much lower speed of ≈ 0.01 mm/min to ensure that full sample drainage took place during shearing and that the test could be interpreted as a drained test. Vertical and horizontal displacements of samples were obtained throughout the test using two LVDT. A dynamometric ring measured the shear force applied in the horizontal plane of failure. The relationship between shear stress (τ) and horizontal displacement was plotted for each vertical stress applied. The cohesion (c') and the friction angle (Φ') of samples were obtained by a regression analysis of the normal and shear stresses corresponding to failure at different values of σ'_v to establish the Mohr-Coulomb failure envelope (Eq. 8). The vertical strain was determined as the measured height variation of samples (Δh) normalized by the initial height (h_0). The average G for dp<2 mm was also considered for IBA-12M, whereas the total average G was used for IBA-3M.

$$\tau_f = c' \times \sigma'_f \times tg(\Phi') \quad (8)$$

Where: τ_f – shear stress, relative to peak or residual conditions; σ'_f – normal effective stress; c' – cohesion; Φ' – friction angle; f and ' represent *failure conditions* and *effective stress*, respectively.

2.3.5. Shear strength and stiffness: triaxial tests

A triaxial test was performed with IBA-12M under consolidated drained (CD) conditions, following the recommendations of ASTM D7181–20. The sample was previously compacted with the w_{opt} from the Proctor test and similar specific energy: 9 layers were compacted in the cylindrical mould with an extension (in order to obtain a sample with a total height of 20 cm), applying 25 hammer falls to achieve the same compaction energy. The sample was covered with a silicone membrane sealed at the top and bottom with o-rings, as commonly done in the triaxial apparatus. Saturation cycles were conducted with upwards water percolation at increasing water pressures until full saturation, which was confirmed through a Skempton coefficient (quotient between the variation of pore water pressure (u) and the variation of confining stress (σ_3), i.e., $\Delta u/\Delta\sigma_3$) above 0.95. Isotropic consolidation was conducted using σ_3= 525 kPa and u = 400 kPa. Thus, the effective confining stress ($\sigma'_3 = \sigma_3 - u$) during the test was 125 kPa. Then, the sample was sheared by increasing the axial deviatoric stress (q), using a vertical strain rate of 0.035 mm/min. According to Le et al. [40], IBA is not meaningfully influenced by the loading rate ranging from 0.009 mm/min to 0.144 mm/min. The σ'_3 and the axial stress ($\sigma'_1 = \sigma'_3 + q$) were used to obtain the Mohr circle in τ-σ'_n graph. The stress-strain ($q - \varepsilon_a$) behaviour was analysed through the Young's modulus (E). For this purpose, the E_0 from the initial slope of the stress-strain curve (q-ε_a), E_{50} from the slope at 50% of the maximum deviator stress, and E_f from the slope at maximum deviator stress (failure) were obtained. These were plotted with other values in E-ε_a graph to assess the so-called stiffness degradation that is usually observed with the axial strain. In fact, even if E_{50} is commonly used in foundation problems [40], other values may be more suitable for other geotechnical problems, including road and railways embankments. Furthermore, the coefficient of permeability (k; in m/s) was obtained applying Darcy's law to a constant-head-induced vertical flow of water on the triaxial sample, through Eqs. 9–12.

$$v = k \times i \quad (9)$$

$$v = \frac{Q}{A} \quad (11)$$

$$Q = \frac{\Delta V}{\Delta t} \quad (10)$$

$$i = \frac{\Delta H}{L} \quad (12)$$

$$\Delta H = \frac{\Delta u}{\gamma_w} \quad (13)$$

Where: v – flow velocity (m/s); i – hydraulic gradient; Q – flow rate (m^3/s); A – cross-sectional area (m^2); ΔV – volume of water flowing through the sample during Δt (m^3); Δt – time variation; ΔH – hydraulic head (m); L – flow distance relative to ΔH (sample height; m); Δu - pore pressure variation relative to ΔH (kPa); γ_w – unit weight of water (= 9.81 kN/m^3).

3. Results and discussion

3.1. Environmental hazard assessment

3.1.1. Chemical characterization

The chemical properties of IBA-3M and IBA-12M (Table 2) and their eluates (Table 3) were generally consistent with the literature (Tables 2 and 3). The OM of both IBA samples was similar and low (Table 2), exhibiting potential for use as a construction material from this viewpoint. Likewise, the natural pH of both samples was similar (Table 3). The pH was in the upper limit of the range of culture media used for organisms tested in ecotoxicological assessment and of tolerance generally assumed for aquatic life (6.5–9) [52], with IBA-12M slightly surpassing this limit. On the other hand, the EC of IBA-3M was one order of magnitude above the one observed for IBA-12M, indicating a higher content of total dissolved solids, consequently, suggesting higher salts leaching potential for IBA weathered for a shorter period of time. Indeed, IBA-3M showed higher concentrations for most elements and ions in its eluate (Table 3). Regarding PTM, the concentration of Cu stands out in the eluates of both samples (while IBA-3M presents a higher concentration) as expected from the literature (Table 3). However, all PTM and ions in both eluates were found in relatively low concentrations and complied with limit values for non-hazardous waste landfills, most of them even complying with limit-values for inert waste landfills. The exceptions to this trend were Cu for IBA-3M and Sb for both eluates. It should be noted that Cu is an essential metal, for example as a cofactor of various enzymes, when below toxic levels [53,54]. Non-ferrous metal recovery from IBA was not performed in the incinerator plant, and the inclusion of this type of treatment (through Eddy current) for consequent recycling of these metals could also reduce their concentration on IBA, potentially decreasing their leaching potential.

Table 2
Chemical characterisation of IBA samples.

Parameter	IBA-3M	IBA-12M	Literature
Moisture (%)	21 ± 2	17 ± 1	7–30[c]
OM (%)	3.6 ± 0.5	3.4 ± 0.9	0.2–5[d]
Elements g/kg			
Ca	54.6 ± 6.08[a]	69.4 ± 6.98[a]	56.3–306[e]
Na	20.6 ± 1.07[a]	17.7 ± 0.83[a]	11.4–57.7[e]
K	7.16 ± 1.01[a]	5.02 ± 0.59[a]	6.89–17.6[e]
Mg	11.6 ± 0.02[a]	12.7 ± 0.24[a]	7.08–30.7[e]
Fe	35.0 ± 0.08[a]	47.0 ± 0.15[a]	14.2–159[e]
P	12.0 ± 1.72[b]	12.0 ± 1.26[b]	2.40–24.0[e]
mg/kg			
Mn	750 ± 0.03[b]	1300 ± 0.05[b]	83–3408[e]
As	14 ± 1.93[b]	17 ± 3.19[b]	0.28–38[e]
Cd	2.9 ± 0.46[b]	7.7 ± 0.46[b]	0.3–146[e]
Co	107 ± 13.2[b]	66 ± 11.2[b]	6–350[e]
Cr	25 ± 13[a]	40 ± 2[a]	21–3170[e]
Cu	1245 ± 14[a]	1308 ± 47[a]	190–12,000[e]
Hg	8 ± 1.31	9 ± 0.28	0.02–8[e]
Ni	35 ± 3[a]	45.0 ± 0.1[a]	7–4280[e]
Pb	2443 ± 96[a]	1095 ± 32[a]	98–13,700[e]
Sb	42 ± 8.50[b]	61 ± 7.29[b]	10–159[e]
V	40 ± 4.32[b]	52 ± 3.26[b]	20–122[e]
Zn	1625 ± 8[a]	2843 ± 106[a]	613–13,600[e]

Bold: PTM;
[a] FAAS;
[b] ICP-MS;
[c] [19,55];
[d] [56];
[e] [27,29,57–75].

Leaching limit values established for IBA use in European countries are mostly above EU leaching limit values for inert landfill, and the permitted application is frequently considered to establish these values [9]. Indeed, thresholds should translate the utilisation conditions of IBA and be established specifically for this material.

3.1.2. Ecotoxicological assessment

Inhibitions of all endpoints assessed were under 50% for all species tested with IBA eluates (Table 4). Thus, no relevant ecotoxic effects were found in the ecotoxicological assessment. Nonetheless, statistically significant effects of leachates were occasionally found (Table S1; supplementary material - SM) that agree with other studies from the literature.

Regarding *A. fischeri*, Römbke et al. [27] also found such low inhibitions (<14%) for seven different samples of weathered IBA, and the same was verified by Ribé et al. [28] for a weathered IBA sample (inhibitions <10% for eluate concentrations <80%). Bandarra et al. [29] observed inhibitions <9.9% for 3 months weathered IBA (< 2 mm). From different elements analysed by Fulladosa et al. [83], an EC_{20} (concentration estimated to elicit 20% of effect) value of 0.26 ± 0.06 mg Cu/L has been estimated for *A. fischeri*, which is under the value measured for IBA-12M. However, IBA is a complex matrix with different components interacting, which may influence ecotoxicity and explain the lack of direct relationships between elemental concentrations and ecotoxic effects. This was also observed by Bandarra et al. [29].

Although ecotoxic effects regarding the growth rate of *R. subcapitata* were not meaningful (or even inexistent), microalgae showed higher sensitivity to IBA-3M (shorter weathering period). Likewise, Stiernström et al. [84] did not observe ecotoxicity for weathered IBA with 3 months and >15 years for *A. fischeri* nor *R. subcapitata*. Such low inhibitions were also found by Römbke et al. [27] for 5 weathered samples (inhibitions <30%). In Bandarra et al. [29], most test solutions promoted growth compared to the control, possibly because of the supplementary nutrient concentration (e.g. K). Although ecotoxic effects were not relevant, the frond number was slightly more sensitive to eluates than the dry weight of *L. minor*, in contrast to Bandarra et al. [29], reinforcing the importance of analysing ecotoxicity with both endpoints. Growth rate inhibitions for macrophytes were higher following exposure to IBA-12M than in microalgae, supporting *L. minor* testing to represent producers in this context, in line with Bandarra et al. [29]. In other studies [43,44] this was even more evident. Conversely, Moser and Römbke [85] found negligible effects (median effect concentration, EC_{50} > 90%) for *L. minor* in 6 out of 10 tests with IBA eluates in an

Table 3
Chemical characterisation of IBA eluates.

Parameter	IBA-3M	IBA-12M	Literature	Inert landfill limit-value[h]	Non-hazardous landfill limit-value[h]
pH[a]	9.0 ± 0.9	9.3 ± 0.7	8–10[e]		
EC[a] (mS/cm)	1.2 ± 0.1	0.32 ± 0.09	1.2–4 [f]		
Elements (mg/kg)					
Ca	499 ± 52[b]	211 ± 39[b]	1500–7500 [g]		
Na	1967 ± 63[b]	748 ± 24[b]	1000–2500 [g]		
K	191.1 ± 0.2[b]	81 ± 12[b]	200–1000 [g]		
Mg	32.5 ± 0.1[b]	0.72 ± 0.03[b]	<5–1000 [g]		
Fe	<0.8[b]	<0.8[b]	0.1–1 [g]		
P	1.37 ± 0.02[c]	2.04 ± 0.02[c]	400–900 [g]		
Mn	0.025 ± 9 × 10^{-6}[c]	0.019 ± 0.001[c]	<0.6 [g]		
As	0.036 ± 0.004[c]	0.085 ± 0.004[c]	0.01–0.05 [g]	0.5	2
Ba	0.13 ± 0.001[c]	0.03 ± 0.002[c]	0.05–1.04 [g]	20	100
Cd	0.0012 ± 0.0002[c]	<0.001[c]	<0.001–0.04 [g]	0.04	1
Cr	0.057 ± 0.001[c]	0.067 ± 0.001[c]	0.03–1.40 [g]	0.5	10
Cu	8.82 ± 0.15[c]	0.93 ± 0.02[c]	0.20–8.22 [g]	2	50
Hg	<0.001[c]	0.0013 ± 0.0001[c]	<0.001–0.05 [g]	0.01	0.2
Mo	0.2 ± 0.004[c]	0.073 ± 0.002[c]	0.085–1.26 [g]	0.5	10
Ni	0.11 ± 0.002[c]	0.017 ± 0.001[c]	<0.001–0.15 [g]	0.4	10
Pb	0.01 ± 0.0002[c]	0.036 ± 0.001[c]	0.003–0.5 [g]	0.5	10
Sb	0.2 ± 0.002[c]	0.18 ± 0.002[c]	0.23–0.39 [g]	0.06	0.7
Se	<0.03[c]	<0.03[c]	<0.001–0.25 [g]	0.1	0.5
Zn	0.094 ± 0.002[c]	0.15 ± 0.003[c]	<0.001–1.7 [g]	4	50
Ions (mg/kg)					
Cl^-	423 ± 6[d]	50 ± 8[d]	239–6700[d]	800	15,000
SO_4^{-2}	281.2 ± 0.3[d]	254 ± 10[d]	175– 9980[d]	1000	20,000

Bold: PTM;
[a] L/S=10 L/kg;
[b] FAAS;
[c] ICP-MS;
[d] Ion chromatography;
[e] Weathered IBA [16,18,29];
[f] Weathered IBA [73,76];
[g] [13,18,27,29,69,73,74,77–82];
[h] Council Decision 2003/33/EC establishing criteria and procedures for the acceptance of waste at landfills.

Table 4
Maximum inhibitions observed for biological endpoints analysed and corresponding eluate concentration for IBA eluates.

Species	IBA-3M		IBA-12M	
	Maximum inhibition (%)	Concentration (%v/v)	Maximum inhibition (%)	Concentration (%v/v)
A. fischeri	13.8	6.25	13.5	6.25
R. subcapitata	16.7	100	-0.04	6.25
L. minor				
Frond number	15.0	100	19.9	100
Dry weight	14.0	12.5	6.8	6.25
D. magna	10.0	100	45.0	100
L. sativum				
Seed germination	6.7	6.25, 50, 100	3.6	3.125
Root growth	4.4	100	9.7	50

international ring test, where microalgae were more sensitive, reflecting the heterogeneity and complexity of the IBA matrix.

D. magna showed higher immobilisation for IBA-12M compared to IBA-3M. This species was the most sensitive regarding IBA-12M, which may have resulted from pH in IBA-12M eluates being slightly above the optimal upper limit indicated in the OECD guideline 202 for this species (pH 9). This effect was previously observed by Bandarra et al. [44], testing coal fly ash with and without pH adjustment. Römbke et al. [27] observed no immobilisation for 2 among 8 samples of weathered IBA, but all samples induced greatly distinct effects and daphnids were the most sensitive aquatic organisms. Likewise, daphnids were considered the most sensitive test species by Ribé et al. [28], possibly due to Cu and Cr concentrations in their IBA eluate (2.87 ± 0.29 and 1.28 ± 0.09 mg/L, respectively), higher than the ones from the present study (Table 3). No relevant ecotoxic effects were observed by Lapa et al. [25] for *D. magna* with IBA eluate with pH 8.9, and *microalgae* were the most sensitive in their case. Bandarra et al. [29] found no immobilisation for weathered IBA with pH = 8.0 ± 0.2.

Similar to Bandarra et al. [29], IBA eluates did not induce relevant ecotoxic effects on seed germination or root growth of *L. sativum*. Eluates of a mineral-organic composite of a mixture of sewage sludge and IBA were previously found to promote the growth of these seeds [86], which was likely linked to non-toxic concentrations of nitrogen compounds and low concentrations of PTM. Another study [87] analysed *L. sativum* exposed to solid fresh and artificially aged IBA, with aged IBA causing no relevant effects, whereas fresh IBA promoted decreasing biomass and increasing germination delay. In this study, the effect of different weathering periods was not noticed for this species.

Thus, both samples could be classified as not ecotoxic. Indeed, weathering is expected to reduce pH and PTM and salts leaching potential, leading to higher stability of IBA in the environment and reducing the potential for negative environmental impacts. Nonetheless, it should be noted that different batches of IBA should be analysed regarding ecotoxicological assessment prior to application given its heterogeneity.

3.2. Geotechnical assessment

3.2.1. Physical characterization

IBA-3M and IBA-12M (as received) displayed wide particle size distribution (Fig. 1), agreeing with the literature [55]. The PI obtained for IBA samples was low (Table 5), indicating low plasticity. This is a good indicator for materials to be applied in pavement bed layers, since high PI may lead to significant layer thickness variations due to water loss or absorption. Sridharan & Gurtug [88] found higher percent swelling for higher LL and PI. According to ASTM D 2487, consistency limits (Table 5), and values of C_C and C_U (Fig. 1) obtained, samples were classified, from the geotechnical point of view as: sand - poorly-graded sand (SP); IBA-3M and M2 - poorly-graded sand with silt (SP-SM); M1 and IBA-12M - well-graded sand with silt (MW-SM). The well-graded nature of M1 derived from mixing poorly-graded IBA-3M (C_C>3) and poorly graded-sand (C_U<6), widening the grain size distribution of both

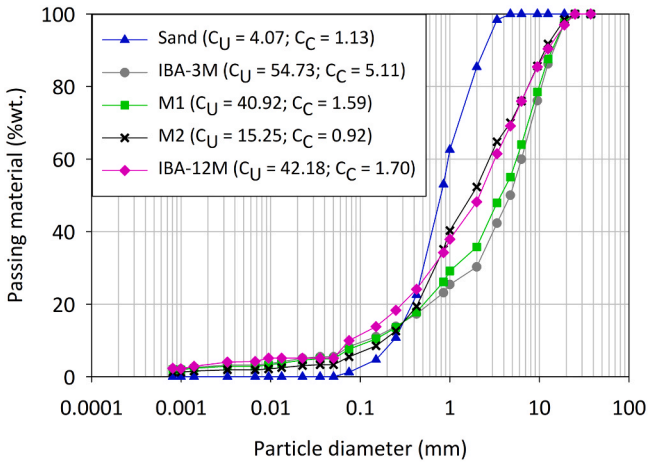

Fig. 1. Particle size distribution of test materials. Coefficients of uniformity (C_U) and curvature (C_C) are given between brackets.M1 – 90% IBA:10% sand; M2 – 60% IBA:40% sand.

Table 5
Solid particles density of different particle size fractions and liquid limit (LL), plastic limit (PL), and plasticity index (PI) of IBA samples.

Parameter	IBA-3M	IBA-12M
G: dp < 0.425	2.63 ± 0.02	2.57 ± 0.07
G: 0.425 ≤ dp ≤ 2.0	2.66 ± 0.01	2.64 ± 0.11
G: 2.0 ≤ dp ≤ 9.5	2.56 ± 0.0004	3.19 ± 0.51
LL (%)	46.2	40.2
LP (%)	42.5	35.9
PI (%)	3.7	4.3

materials. The G obtained for sand was 2.60 ± 0.12, which is a common value that reflects the composition of the grains (mostly silica). For IBA-12M, a higher G was found for coarser particles (>2 mm) (Table 5), probably due to its heterogeneous composition between fractions. Indeed, finer fractions have been found to have more uniform composition [89]. Nonetheless, the average G for IBA-3M and IBA-12M was 2.62 ± 0.05 and 2.8 ± 0.3, respectively, which are within the expected range (1.2–2.8) [55]. Hence, G=2.62 and G=2.61 were estimated for M1 and M2, respectively. All values agreed with the foreseen range for most soils (2.60–2.80) [90].

3.2.2. Compaction: modified Proctor test

Compaction curves of IBA-3M, M2, and IBA-12M (Fig. 2) are qualitatively similar to the ones of soils usually used in embankments, although the shape of the curve for M2 seemed to be affected by the presence of relatively uniform sand which exhibits atypical compaction curves without a well-defined peak. The compaction curves of all samples plot to the left of the zero-air-void curve (S=100%), validating the

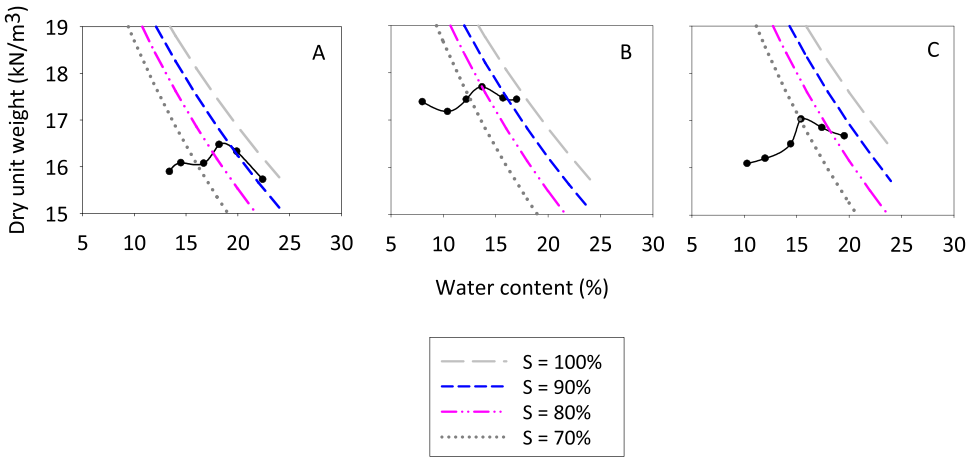

Fig. 2. Compaction results from the Proctor test for A) IBA-3M, B) M2, and C) IBA-12M. S: degree of saturation.

experiments (Fig. 2). For IBA-3M, w_{opt} = 18.2% and γ_{dmax} = 16.48 kN/m^3 (Fig. 2A) were obtained. In the case of M2, w_{opt} and γ_{dmax} were 13.7% and 17.70 kN/m^3 (Fig. 2B), respectively, indicating better compaction and lower water content when mixing IBA with sand. The addition of sand decreased the impact of the fine fraction, certainly presenting higher plasticity, and complemented the granulometric distribution of IBA. Coarser soils tend to display lower w_{opt} and higher γ_{dmax} [91]. Regarding IBA-12M, w_{opt} = 15.4% and γ_{dmax} = 17.03 kN/m^3 were estimated. These results agree with the literature. Values of w_{opt} from 9.6% to 20% and γ_{dmax} from 12.16 to 18.04 kN/m^3 were indicated for IBA by Chandler et al. [69]. Similarly, Lynn et al. [92] presented w_{opt} from 12% to 18% and γ_{dmax} from 11.77 to 17.65 kN/m^3. IBA-12M showed lower w_{opt} and higher γ_{dmax} than IBA-3M, reflecting better compaction conditions, namely a coarser nature of the grains and a plasticity reduction induced by weathering. Compaction is usually applied for embankments construction and other geotechnical applications. Thus, these conditions were used in the following assays to assess the mechanical behaviour of samples under the specific conditions of a real application scenario.

3.2.3. *One-dimensional compressibility: oedometer test*

The w obtained for M1, IBA-3M and M2 after compaction (Table S2,

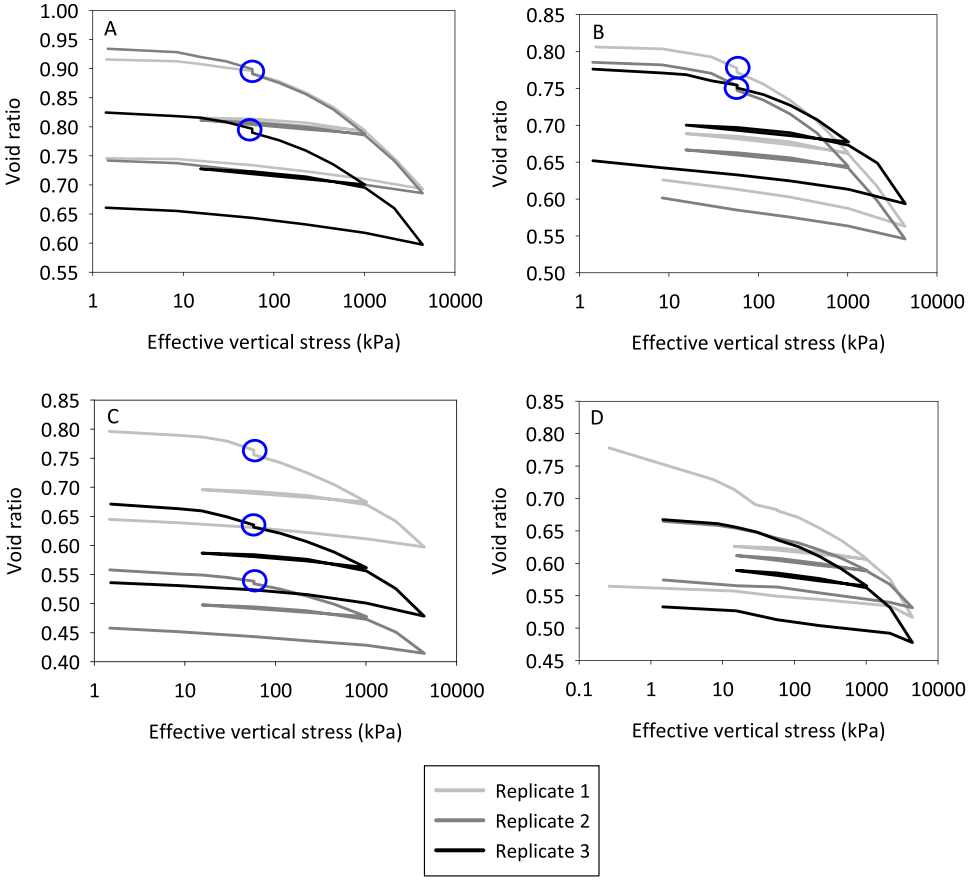

Fig. 3. Void ratio as a function of effective vertical stress (kPa) obtained in the oedometer test for A) IBA-3M, B) M1, C) M2, and D) IBA-12M. The blue circles indicate minor collapses due to saturation.

SM) were similar to the corresponding values of w_{opt}, as expected (Section 3.2.2). The γ_d of all the samples substantially differed among themselves and from the corresponding value obtained in the Proctor test. These differences may result from several factors, e.g., different size fraction used to attend to the size of the oedometer ring, heterogeneity of materials and differences in the compaction method adopted because of maximum sample size. However, the results from this study are relevant since they are obtained with a less rigid material (due to the lower γ_d) than the one obtained in the field, thus yielding conservative values.

The e-log σ'_v curves obtained for all samples (Fig. 3) show a smooth shape, indicating there was no meaningful particle crushing at any stress level [93,94]. The discrepancy of e_0 of replicate 3 of IBA-12M regarding the others (Fig. 3A) may be related to the preparation process, demonstrating the difficulty in preparing uniform replicates, or to difficulties in experimentally evaluating the value of e_0 more accurately (saturation problems, bedding errors, etc). The difference between e_0 (σ'_v= 1.5 kPa) and the final e at the highest effective stress (σ'_v=4424 kPa) for all replicates is 0.23 ± 0.02, and thus very similar. Closer values of e_0 were found for replicates of M1, indicating better sample preparation. The variation between e_0 and e at the highest effective stress was 0.22 ± 0.03. This variation was slightly lower for replicate 3, showing an atypical behaviour for higher stresses. M2 was the sample presenting the greatest discrepancy regarding e_0 among replicates possibly due to the increased difficulty of preparing samples with significant proportions of two different materials, due to segregation effects. The difference between e_0 and e at the highest effective stress for M2 was 0.18 ± 0.03. Regarding IBA-12M, replicate 1 showed different behaviour compared to the others, showing an unexpected curve at low stresses, probably because of an initial bedding error of the loading arm possibly increased by the lower γ_d. The variation between e_0 and e at the maximum vertical stress was 0.14 ± 0.06. Replicate 1 showed higher variation, though results would be similar if the bedding error was corrected. A very slight collapse (<0.01) was observed with the addition of water for all samples, except for IBA-12M, the minor effects observed not representing any negative impact in real conditions. Swelling was not observed in any of the replicates.

Relevant differences were found among samples for the compression index, but not regarding the recompression index (Table 6). IBA-3M and M1 presented similar C_c, but M2 showed slightly lower C_c, suggesting lower compressibility due to higher proportion of sand. Simultaneously, IBA-12M displayed lower C_c compared to IBA-3M and similar to M2, although slightly higher than the latter. This may suggest a stiffer behaviour under unidimensional loading for IBA with longer weathering period, and/or be related to IBA heterogeneity. The C_r/C_c ratio of all samples was around 1/12, which is near the typical range for soils (1/10–1/5) [90], and is similar to other IBA samples and mixtures [29]. Consolidation occurred very quickly at each new load, as the permeability of the tested materials significantly exceed that of clayey soils that are commonly tested in the oedometer test. Only the load level corresponding to 452 kPa was used to determine Cv, considering Taylor method requirements. As expected, the values of Cv and k increased with the presence of sand and its proportion in comparable mixtures (Table 6). After compaction, all materials presented reasonable permeability values, with IBA-12M presenting the higher permeability. Raju et al. [95] found a relationship between LL and k, in which k increases with decreasing LL. This is a possible explanation for the results obtained for IBA-12M (<LL; Table 5). The results obtained in this work are closer to the typical permeability of fine sand/loose silt (10^{-7}–10^{-5} m/s) [96]. Gupta et al. [33] found C_c=0.04–0.07 and k from 8×10^{-6} to 1×10^{-5} m/s for IBA. C_c values from this work were higher than those but were within the range for sand from the literature: 0.002–1 for an effective vertical stress range of 0.001–1000 MPa [97]. Likewise, C_r values were consistent with the literature for sand: 0.0023–0.0150 for maximum vertical stress of 300 kPa [98]. The k values for IBA-12M and M2 were consistent with Gupta et al. [33], but the remaining samples were not. Gupta et al. [33] studied IBA from India, which presents a different economic and cultural context, and thus IBA composition may significantly differ from IBA from this work, possibly explaining differences found. Furthermore, the maximum applied stress was below 1000 kPa, under the ones applied in this work. Le et al. [34] obtained $C_c = 0.046 \pm 2.8\times10^{-4}$ and $C_s = 0.0036 \pm 7.1\times10^{-5}$ for compacted immersed IBA with a maximum stress of 6613 kPa. However, the e_0 was much lower (approximately 0.43), possibly explaining the lower compressibility. Previous work [29] with non-compacted IBA applying similar effective stresses resulted in C_c=0.405 ± 0.07 and C_r=0.029 ± 0.001. The same study found C_c=0.241 ± 0.01 and C_r = 0.022 ± 0.01 for a non-compacted mixture with sand (70%). In this study, compressibility was much lower as expected given the compaction step in sample preparation. Likewise, Le et al. [34] showed that compacted IBA was less compressible, while non-compacted IBA was highly compressible. For applications such as road embankments, the compaction of materials ensures a much-required reduction of compressibility.

Table 6
Coefficients calculated from the oedometer test (average ± standard deviation).

Sample	C_c	C_r	C_v (m^2/d)	k (m/s)
IBA-3M	0.182 ± 0.017	0.013 ± 0.001	80.14 ± 29.16	$5.40\times10^{-7} \pm 1.90\times10^{-7}$
M1	0.172 ± 0.005	0.013 ± 0.001	107.57 ± 58.61	$6.13\times10^{-7} \pm 3.82\times10^{-7}$
M2	0.136 ± 0.018	0.012 ± 0.002	155.48 ± 75.33	$1.04\times10^{-6} \pm 3.21\times10^{-7}$
IBA-12M	0.155 ± 0.044	0.012 ± 0.001	828.62 ± 572.06	$4.68\times10^{-6} \pm 3.66\times10^{-6}$

3.2.4. Shear strength: shear box test

The values of w_{opt} and γ_d replicated well with the adopted compaction method. Nonetheless, the values obtained (Table S3; SM) do not correspond to the Proctor test values (particularly γ_d), being lower than the ones from the oedometer test. Sample compaction was performed differently in this case, due to its geometry (Section 2.3.4), which may have contributed to these divergences. The hammer fell directly on an iron cube, which may not allow to properly replicate the compaction energy of the Proctor test. The curves that relate the shear stress (τ) with horizontal displacement (Fig. 4 A-D.i.) obtained for all samples are typical of dense soils [99]. The same occurred for the normalized stress-strain curves (Fig. 4 A-D.ii.), where the effect of vertical (normal) stress is evident, as observed in dense granular soils, i.e., the relative value of the peak shear strength in relation to the residual shear strength increases with decreasing normal stress. Moreover, the curves of vertical strain as a function of horizontal displacement obtained (Fig. 4 A-D.iii.) were also typical of dense granular materials, since the samples expanded significantly after an initial compression phase during shear to allow the formation of the failure plane.

As expected, peak shear stress (τ_{peak}) and residual shear stress (τ_{res}) increased with increasing σ'_n (Fig. 5). Compacted specimens usually display different peak and residual shear strength values for the same σ'_n, the former relating to the maximum shear stress that materials can tolerate and the latter to the shear strength mobilized at large strains, which are used as reference in different scenarios. The parameters of shear strength in terms of effective stresses, namely the cohesion (c') and the friction angle (Φ'), were determined both under peak and residual conditions (Table 7) based on the linear regressions obtained from plotting the τ_{peak} and the τ_{res} as a function of σ'_v (=σ'_n) for each sample (Fig. 5).

The cohesion of IBA-3M decreased with the increasing percentage of sand (M1, M2) under peak conditions, while the mixture with sand does not seem to have a relevant effect regarding the friction angle. The c' value of IBA-3M regarding its mixtures may arise from the elongated particles crossing the horizontal shear plane, hence increasing the shear resistance at low normal stresses. Moreover, IBA-12M presented the lower c' and the higher Φ' (especially Φ'_{peak}) from all samples tested.

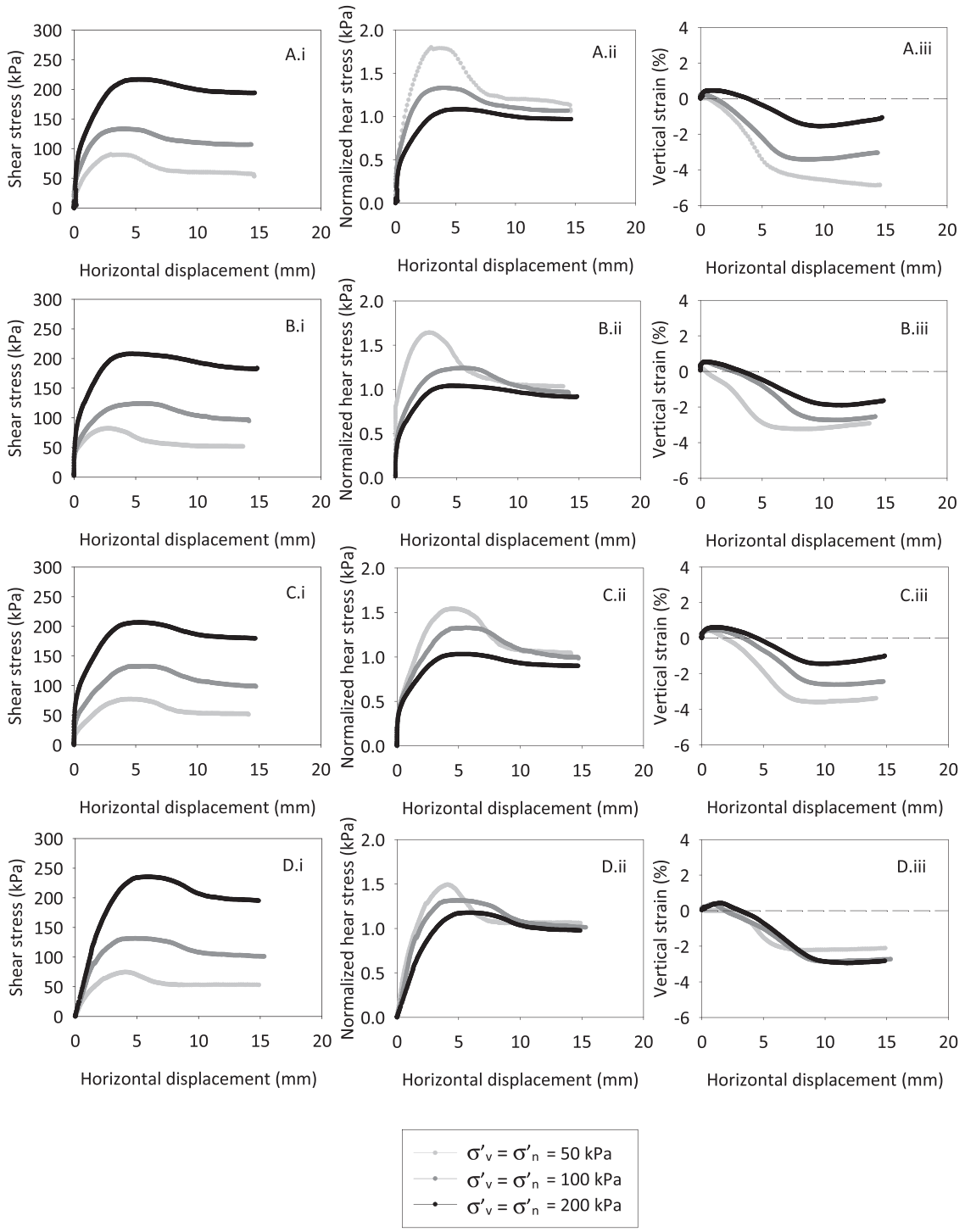

Fig. 4. Shear stress (i), normalized shear stress (ii), and vertical strain (iii) as a function of horizontal displacement for (A) IBA-3M, (B) M1, (C) M2, and (D) IBA-12M.

The results were similar in residual conditions, except for the expected reduction in cohesion compared to peak conditions. In fact, c' was expected to be closer to zero in non-cemented granular materials [100]. However, the non-zero cohesion under peak conditions can be possibly explained by the non-linearity of the Mohr-Coulomb envelope typically observed for lower stress levels in dense granular materials. This non-linearity of the failure envelope results in a non-zero value of c' that has no physical meaning.

The greater the friction angle, the more resistant the material. In previous work [29], c'_{peak}=16.2 kPa and Φ'_{peak}=32° were obtained for loose IBA and c'_{peak}=9.9 kPa and Φ'_{peak}=36.1° for a loose mixture with sand (70%). Thus, the compacted sample from this study showed higher shear strength, as expected. Gupta et al. [33] found Φ'_{peak} =43.3–49.7° and Φ'_{res}=36.5–40.3° for IBA at normal stress of 100, 200 and 400 kPa, which is close to the results from this work. Another study [38] analysed a sample under normal stresses of 5.5, 11, and 16.2 kPa and found a slightly lower c'_{peak} of 9.6 kPa and a slightly higher Φ'_{peak} of 50.2°, probably because the tests focused on the non-linear part of the failure envelope. Overall, values found for Φ' for all samples of this work were within the range for peak shear strength (30–48°) for dense granular soils and higher than the ones found for their residual shear strength (26–36°) in the literature [101], possibly due to the irregular shape of

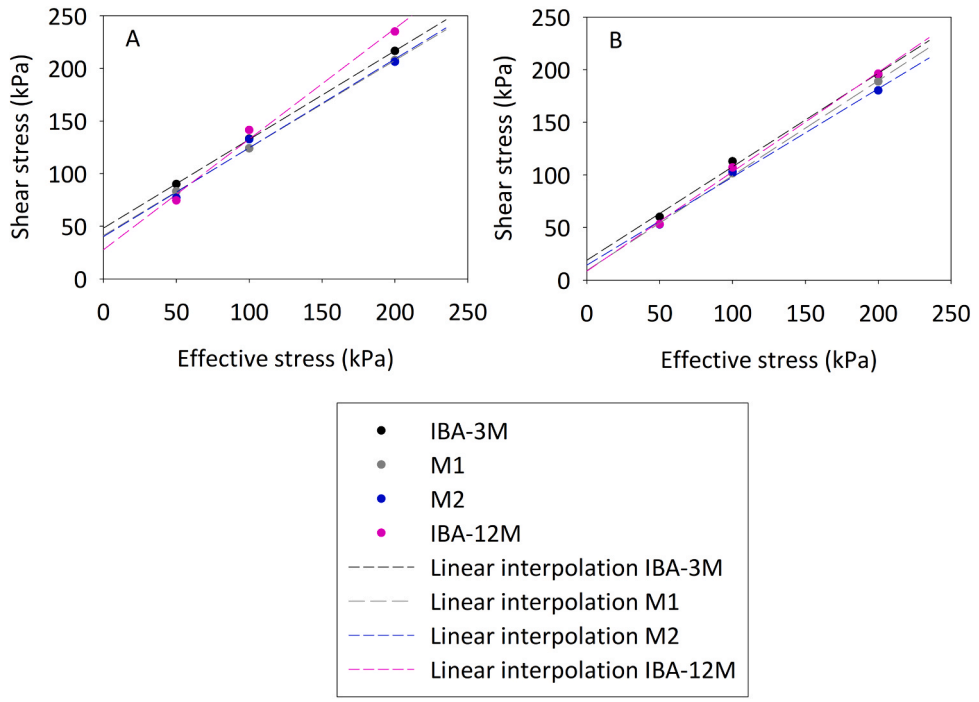

Fig. 5. Mohr-Coulomb failure envelopes for IBA-3M, M1, M2, and IBA-12M at (A) peak and (B) residual conditions.

Table 7
Shear strength properties of tested material obtained from the shear box test.

Sample	σ_v' (kPa)	τ_{peak} (kPa)	c'$_{peak}$ (kPa)	Φ'$_{peak}$ (°)	τ_{res} (kPa)	c'$_{res}$ (kPa)	Φ'$_{res}$ (°)
IBA-3M	50	90.0	46.2	40.1	60.0	18.9	41.6
	100	133.0			112.8		
	200	216.5			194.9		
M1	50	83.1	41.2	39.8	52.8	9.1	42.0
	100	124.0			101.5		
	200	207.7			188.8		
M2	50	77.0	40.2	40.2	52.9	14.2	40.0
	100	132.6			102.9		
	200	206.2			180.3		
IBA-12M	50	74.5	27.7	46.4	53.1	8.5	43.4
	100	141.4			107.0		
	200	234.9			196.1		

the particles and the rough nature of their surfaces. Thus, all materials have similar behaviour to that of compact granular materials, such as those that are generally used to embankments. IBA-3M and its mixtures with sand showed slightly higher shear strengths for lower effective stress (<50 kPa), while IBA-12M presented higher shear strength for greater effective stress. Possibly the well-graded nature of IBA-12M (Section 3.2.1) and the reduced plasticity induced by weathering may contribute to explain these results. Nonetheless, all the samples presented good shear strength at peak and residual conditions. Because sand had a minor impact on shear strength of IBA, from this perspective IBA may be applied alone, potentially reducing its landfilling and the extraction of larger amounts of raw material in line with the circular economy goals. Globally, the results suggest that IBA and the tested mixtures present significant shear strength, hence revealing potential for field applications where the loading conditions are challenging.

Since IBA presented lower permeability than mixtures, potentially presenting slower drainage during shear, an additional test was conducted at lower strain rate to evaluate the possible effect of positive or negative excess-pore-pressure generation in case the selected shear speed did not allow for total drainage in the shearing zone. The test was performed for σ'_v=100 kPa. Shearing-induced positive or negative excess-pore water pressure can affect soil strength, both in the field and in laboratory tests, namely when the equipment is unable to measure these variations. In particular, slopes stability resulting from increasing shear strength promoted by suction may be threatened if the pore water pressure increases [102]. In this case, the sample response at significantly different shear strain rates was very similar, demonstrating that there was no excess-pore-pressure generation effect in any of the tests (Fig. S1, SM). Thus, the tests were performed under strictly drained conditions as initially predicted.

3.2.5. Shear strength and stiffness: triaxial test

The Mohr circle obtained from the triaxial test for IBA-12M at peak conditions (Fig. 6A) shows that a slightly larger shear strength was found compared to the one derived from the shear box test. This is mostly a result from the fact that a better compaction was obtained in sample preparation in this case. In fact, w_{opt} = 15.4% and γ_{dmax} = 16.28 kN/m^3 were obtained in compaction carried out for the triaxial test, which is closer to the values obtained for the Proctor test. As previously mentioned, compaction for the shear box test was carried out by hammering an iron cube, while the compaction method used for the triaxial test was much closer to the one from the Proctor test, which is clearly more effective. Moreover, the triaxial test was performed with larger particle sizes, which should also probably result in a larger shear strength. Nonetheless, shear strength from both tests seems not to differ significantly. In fact, the results obtained for residual conditions (Fig. 6B) show that shear strength is similar in both tests since the Mohr-Coulomb failure envelope derived from the shear box tests is only slightly above the Mohr circle representing the triaxial stresses at failure. This minor difference could be expected, due to the fact that the failure plane is imposed in the shear box tests while being the weakest in the triaxial test. Compaction should not influence shear strength at very large strains, thus reinforcing that differences found at peak conditions were most probably influenced by the compaction method. Becquart et al. [32] and Le et al. [40] found higher friction angles (Φ'_{peak}= 58.9° and $\Phi'_{residual}$=55.4° in the first case; Φ'_{peak}= 54.51° in the second case) for IBA through CD triaxial tests. However, it should be noted that sample

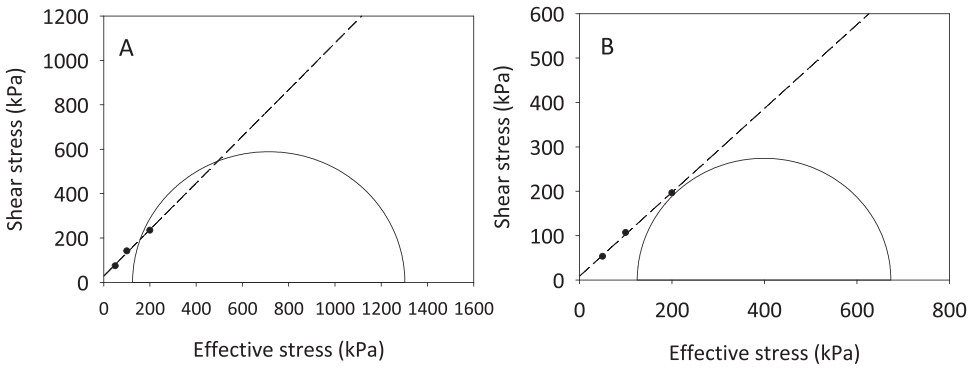

Fig. 6. Mohr-Coulomb failure envelope (shear box test) and Mohr circle (triaxial test) for IBA-12M at (A) peak and (B) residual conditions.

was prepared in a mould with diameter = 101.5 mm and height = 117.5 mm. Thus, the height/diameter ratio of the samples from those studies was about 1.16, which is well below the geometry recommended for triaxial tests (height/diameter ratio of 2) [101]. It should be noted that lower height/diameter ratio tends to result in unrealistic higher samples resistance, because the boundary conditions at the top and bottom of the samples limit their ability to deform during shearing.

With respect to the shear-strain (q-ε$_a$) response (Fig. 7A), IBA-12M showed a behaviour that differs from that usually observed in granular materials under drained monotonic shearing [103]. In fact, the slope of the shear-strain curve shows an atypical reversion of the slope variation with strain, possibly reflecting some minor grain crushing at relatively low strains. As a result, the E-ε$_a$ curve (Fig. 7B) showed an atypical shape compared to soils commonly used in road embankments, which exhibit a continuous stiffness degradation (assessed through the elastic modulus, E) with the shear strain [104]. In contrast, in the triaxial test carried out on IBA-12M, an initial degradation was observed (Fig. 7C) but quickly E increased before it decreased, reaching an unusual peak at a strain exceeding that corresponding to 50% of the peak deviator stress (Fig. 7B). This is possibly due to the breakage of less resistant materials present in IBA. Values of 36.3, 46.0, and 41.2 MPa were obtained for E_0, E_{50} and E_f, respectively, E_0 representing the initial value measured in the triaxial test. The E_{50} value obtained was similar to those found for dense sands (50–80 MPa) [32]. Noteworthy is that the E_{50} from the present study was obtained with a low effective confining stress. Le et. al [40] carried out two sets of triaxial tests and obtained E_{50} of 42.56 MPa for σ'_3= 100 kPa (σ_3 = 300 kPa; u = 100 kPa) and q_{peak} = 1215 kPa, while E_{50} of 48.71 MPa was found for σ'_3= 100 kPa (σ_3 = 500 *kPa*; u = 400 kPa) and q_{peak} = 1357 kPa. These values are close to the one obtained in this work. The order of magnitude of E suggests that compacted IBA presents a good stiffness under triaxial loading [40]. From the unloading/reloading cycle in the shear-strain response, an unloading-reloading E of 162.93 MPa was calculated, which are above the values obtained in the E-ε$_a$ curve but may better represent the real value of E_0 for very small strains, which are difficult to measure in a triaxial test without internal strain measurements and/or wave propagation methods.

Regarding the permeability, $k = 0.8 \times 10^{-6}$ m/s was obtained in this test. The small difference from the value obtained in the oedometer test may be linked to k being obtained indirectly in the latter, using the value of Cv which presents difficulties regarding its experimental determination. Nonetheless, the values determined in both cases are very close, considering the range of variation of k in soils. This difference is also potentially related to different compaction methods, with the one used for the triaxial test being much closer to the one from the Proctor test, as aforementioned.

4. Conclusions

The potential of IBA and mixtures with sand for safe application in geotechnical works (such as road embankments) was evaluated, considering its mechanical and environmental behaviour.

From the chemical viewpoint, a low leaching potential of potentially toxic metals and ions was observed for IBA, complying with limit values for non-hazardous waste landfills, which is the most used application criterion regarding chemical analysis. Concerning ecotoxicity, the

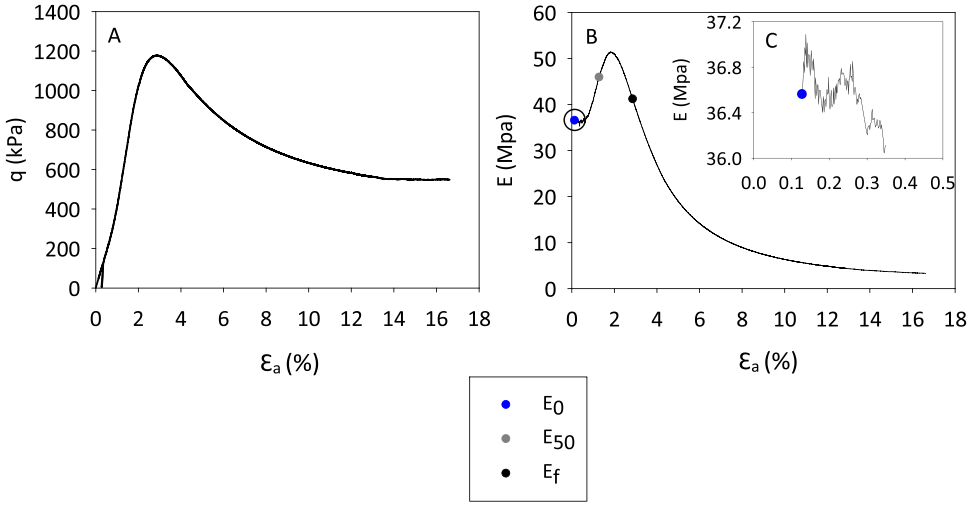

Fig. 7. A) Evolution of deviator stress (q) and B) Young modulus (E) as a function of the axial strain (ε_a). The circle in B) indicates the area of the graph that was zoomed in to better analyse C) the initial elastic behaviour of the sample.

biotest battery was consistent and no relevant toxic responses were identified, suggesting that the tested IBA is non-ecotoxic.

IBA-12M was similar to well-graded sand with silt concerning particle size distribution, while the grain size distribution of the poorly-graded IBA-3M (C_c>3), was widened by mixing it with poor-graded sand (C_U<6). The average G of all materials agrees with the expected range for most soils. Low plasticity and low organic matter was found for IBA samples, showing potential for use in geotechnical works from this viewpoint. Indeed, organic matter content may affect the compressibility and strength of the construction.

M2 presented better compaction behaviour than IBA-3M (Proctor test), suggesting that the addition of sand may enhance compaction, probably linked to the reduced effect of the fine fraction and to a wider grain size distribution. Simultaneously, IBA-12M showed better compaction than IBA-3M, demonstrating once again IBA heterogeneity. The geochemical transformations during IBA weathering may also be a relevant factor. Concerning oedometer tests, the addition of sand to IBA-3M (M1 and M2) decreased its compressibility, although differences found were not substantial. Similarly, IBA-12M presented lower compressibility than IBA-3M, suggesting that weathering may reduce compressibility. All materials presented small settlements and results suggest good one-dimensional stiffness. After compaction, all materials presented permeability values typical of fine sand/loose silt (>IBA-12M). Furthermore, none of the materials showed relevant effects of submersion under load, with no significant collapses or expansions being observed. The results obtained for all samples in shear box tests were qualitatively similar to materials commonly used in geotechnical works, namely dense granular soils. IBA-3M, M1, and M2 showed slightly higher shear strengths for lower effective stresses (<50 kPa), whereas IBA-12M presented higher shear strength for greater effective stresses. However, all samples presented good shear strength. Sand did not significantly affect IBA shear strength. The results from the triaxial test conducted on IBA-12M showed that shear strength was similar to that observed in the shear box test, minor differences being justified by sample preparation methods and particular characteristics of the tests. The permeability coefficient measured in the triaxial test was also similar to the one measured in the oedometer test, highlighting the validation of results. Moreover, the values of the elastic modulus of IBA were close to those shown by materials typically used for road construction. Overall, the ageing period seems to positively influence IBA geotechnical properties. Thus, IBA presented good mechanical behaviour and, consequently, potential to be used as alternative to less noble materials increasingly used in sustainable geotechnical solutions, namely if a period of weathering is allowed.

Globally, IBA samples showed potential both at a technical and environmental level for application as a sustainable construction material in geotechnical works, including embankments and road layers. IBA use ensuring technical quality and environmental protection reduces waste landfilling and natural resources extraction, promoting sustainability and the circular economy. The utilization as construction material seems to be a good option for IBA given the required volumes and technical quality. Specific applications should comprise the evaluation of different batches given IBA heterogeneity. Future work should include the development of a sample preparation method that can improve the replication of the initial conditions and allow a better comparison between tests. Testing mixtures of IBA with other waste regarding its potential for safe use in applications using high amounts of material might be also interesting to maximize the circular economy concept in practice. Finding solutions to increase resource efficiency is extremely relevant in all fields, particularly in the construction sector, where materials are used and disposed of at increasing rates. Noteworthy is scale testing should be considered for specific applications for analysis of materials in the field.

CRediT authorship contribution statement

B.S.Bandarra: Conceptualization, Data curation, Formal analysis, Investigation, Methodology, Validation, Writing – original draft. **L. Monteiro:** Data curation, Investigation, Validation, Writing – review & editing. **G. Veloso:** Data curation, Investigation, Validation, Writing – review & editing. **P. Abreu:** Data curation, Investigation, Validation, Writing – review & editing. **H.Sousa:** Data curation, Investigation, Validation, Writing – review & editing. **R.C.Martins:** Conceptualization, Methodology, Resources, Supervision, Writing – review & editing; **J.L.Pereira:** Conceptualization, Methodology, Resources, Supervision, Writing – review & editing. **P.A.L.F. Coelho:** Conceptualization, Methodology, Resources, Supervision, Writing – review & editing. **M.J. Quina:** Conceptualization, Methodology, Resources, Supervision, Writing – review & editing.

Declaration of Competing Interest

The authors declare that they have no known competing financial interests or personal relationships that could have appeared to influence the work reported in this paper

Data availability

The authors are unable or have chosen not to specify which data has been used.

Acknowledgements

Thanks are due to FCT/MCTES for their financial support to CERES (UIDB/00102/2020) and CESAM (UIDP/50017/2020 + UIDB/50017/2020 + LA/P/0094/2020) through national funds. B.S.B. is the recipient of an individual research grant by the FCT/MCTES with the reference SFRH/BD/147920/2019, through national funds and ESF (European Social Fund).

Appendix A. Supporting information

Supplementary data associated with this article can be found in the online version at doi:10.1016/j.conbuildmat.2024.136011.

References

[1] S. Kaza, L. Yao, P. Bhada-Tata, F. Van Woerden, What a waste 2.0: a global snapshot of solid waste management to 2050, World Bank Publications, 2018. ISBN 9783642253874.
[2] Eurostat Municipal waste by waste management operations Available online: ⟨https://ec.europa.eu/eurostat/databrowser/view/ENV_WASMUN/default/table?lang=en⟩ (accessed on May 14, 2023).
[3] Eurostat Municipal waste landfilled, incinerated, recycled and composted, EU, 1995-2021 Available online: ⟨https://ec.europa.eu/eurostat/statistics-explained/index.php?title=File:Municipal_waste_landfilled,_incinerated,_recycled_and_composted,_EU,_1995-2021.png⟩ (accessed on May 12, 2023).
[4] E. Toraldo, S. Saponaro, A. Careghini, E. Mariani, Use of stabilized bottom ash for bound layers of road pavements, J. Environ. Manag. *121* (2013) 117–123, https://doi.org/10.1016/j.jenvman.2013.02.037.
[5] C.J. Lynn, G.S. Ghataora, R.K. Dhir OBE, Municipal incinerated bottom ash (MIBA) characteristics and potential for use in road pavements, Int. J. Pavement Res. Technol. *10* (2017) 185–201, https://doi.org/10.1016/j.ijprt.2016.12.003.
[6] Crillesen, K.; Skaarup, J.; Bojsen., K. *Management of Bottom Ash from WTE Plants - An overview of management options and treatment methods*; Copenhagen, Denmark, 2006;
[7] J.M. Chimenos, M. Segarra, M.A. Fernández, F. Espiell, Characterization of the bottom ash in municipal solid waste incinerator, J. Hazard. Mater. *64* (1999) 211–222, https://doi.org/10.1016/S0304-3894(98)00246-5.
[8] CEWEP - Confederation of European Waste-to-Energy Plants. Bottom Ash Factsheet. Available online: ⟨http://www.cewep.eu/2017/09/08/bottom-ash-factsheet/⟩ (accessed on Mar 11, 2020).
[9] D. Blasenbauer, F. Huber, J. Lederer, M.J. Quina, D. Blanc-Biscarat, A. Bogush, E. Bontempi, J. Blondeau, J.M. Chimenos, H. Dahlbo, et al., Legal situation and current practice of waste incineration bottom ash utilisation in Europe, Waste Manag *102* (2020) 868–883, https://doi.org/10.1016/j.wasman.2019.11.031.

[10] X. Dou, F. Ren, M.Q. Nguyen, A. Ahamed, K. Yin, W.P. Chan, V.W.C. Chang, Review of MSWI bottom ash utilization from perspectives of collective characterization, treatment and existing application, Renew. Sustain. Energy Rev. *79* (2017) 24–38, https://doi.org/10.1016/j.rser.2017.05.044.

[11] B. Verbinnen, P. Billen, J. Van Caneghem, C. Vandecasteele, Recycling of MSWI bottom ash: a review of chemical barriers, engineering applications and treatment technologies, Waste Biomass-.-. Valoriz. *8* (2017) 1453–1466, https://doi.org/10.1007/s12649-016-9704-0.

[12] G. Weibel, U. Eggenberger, D.A. Kulik, W. Hummel, S. Schlumberger, W. Klink, M. Fisch, U.K. Mäder, Extraction of heavy metals from MSWI fly ash using hydrochloric acid and sodium chloride solution, Waste Manag *76* (2018) 457–471, https://doi.org/10.1016/j.wasman.2018.03.022.

[13] R. del Valle-zermeño, J.M. Chimenos, J. Giró-paloma, J. Formosa, Use of weathered and fresh bottom ash mix layers as a subbase in road constructions: environmental behavior enhancement by means of a retaining barrier, Chemosphere *117* (2014) 402–409, https://doi.org/10.1016/j.chemosphere.2014.07.095.

[14] H. Luo, Y. Cheng, D. He, E.H. Yang, Review of leaching behavior of municipal solid waste incineration (MSWI) ash, Sci. Total Environ. *668* (2019) 90–103, https://doi.org/10.1016/j.scitotenv.2019.03.004.

[15] A. Maldonado-Alameda, J. Giro-Paloma, A. Svobodova-Sedlackova, J. Formosa, J. M. Chimenos, Municipal solid waste incineration bottom ash as alkali-activated cement precursor depending on particle size, J. Clean. Prod. *242* (2020) 118443, https://doi.org/10.1016/j.jclepro.2019.118443.

[16] J.M. Chimenos, A.I. Fernández, R. Nadal, F. Espiell, Short-term natural weathering of MSWI bottom ash, J. Hazard. Mater. *79* (2000) 287–299, https://doi.org/10.1016/S0304-3894(00)00270-3.

[17] R.V. Silva, J. de Brito, C.J. Lynn, R.K. Dhir, Environmental impacts of the use of bottom ashes from municipal solid waste incineration: a review, Resour. Conserv. Recycl. *140* (2019) 23–35, https://doi.org/10.1016/j.resconrec.2018.09.011.

[18] À. Maldonado-Alameda, J. Giro-Paloma, A. Alfocea-Roig, J. Formosa, J. M. Chimenos, Municipal solid waste incineration bottom ash as sole precursor in the alkali-activated binder formulation, Appl. Sci. *10* (2020) 4129, https://doi.org/10.3390/APP10124129.

[19] A.M. Joseph, R. Snellings, P. Van den Heede, S. Matthys, N. De Belie, The use of municipal solid waste incineration ash in various building materials: a Belgian point of view, Mater. (Basel) *11* (2018), https://doi.org/10.3390/ma11010141.

[20] S. Stiernström, O. Wik, D. Bendz, Evaluation of frameworks for ecotoxicological hazard classification of waste, Waste Manag *58* (2016) 14–24, https://doi.org/10.1016/j.wasman.2016.08.030.

[21] P. Pandard, J. Römbke, Proposal for a "Harmonized" strategy for the assessment of the HP 14 property, Integr. Environ. Assess. Manag. *9* (2013) 665–672, https://doi.org/10.1002/ieam.1447.

[22] B.S. Bandarra, S. Silva, J.L. Pereira, R.C. Martins, M.J. Quina, A study on the classification of a mirror entry in the European list of waste: incineration bottom ash from municipal solid waste, Sustainability *14* (2022) 10352, https://doi.org/10.3390/su141610352.

[23] B.M. Wilke, F. Riepert, C. Koch, T. Kühne, Ecotoxicological characterization of hazardous wastes, Ecotoxicol. Environ. Saf. *70* (2008) 283–293, https://doi.org/10.1016/j.ecoenv.2007.10.003.

[24] B. Ferrari, C.M. Radetski, A.M. Veber, J.F. Ferard, Ecotoxicological assessment of solid wastes: a combined liquid- and solid-phase testing approach using a battery of bioassays and biomarkers, Environ. Toxicol. Chem. *18* (1999) 1195–1202, https://doi.org/10.1897/1551-5028(1999)018<1195:EAOSWA>2.3.CO;2.

[25] N. Lapa, R. Barbosa, J. Morais, B. Mendes, J. Méhu, J.F. Santos Oliveira, Ecotoxicological assessment of leachates from MSWI bottom ashes, Waste Manag *22* (2002) 583–593, https://doi.org/10.1016/S0956-053X(02)00009-0.

[26] H. Moser, J. Römbke, Ecotoxicological characterization of waste - Results and experiences of a European ring test, Springer Ltd., New York, USA, 2009.

[27] J. Römbke, T. Moser, H. Moser, Ecotoxicological characterisation of 12 incineration ashes using 6 laboratory tests, Waste Manag *29* (2009) 2475–2482, https://doi.org/10.1016/j.wasman.2009.03.032.

[28] V. Ribé, E. Nehrenheim, M. Odlare, Assessment of mobility and bioavailability of contaminants in MSW incineration ash with aquatic and terrestrial bioassays, Waste Manag *34* (2014) 1871–1876, https://doi.org/10.1016/j.wasman.2013.12.024.

[29] B.S. Bandarra, C. Mesquita, H. Passos, R.C. Martins, P.A.L.F. Coelho, J.L. Pereira, J. Quina, An integrated characterisation of incineration bottom ashes towards sustainable application: physicochemical, ecotoxicological, and mechanical properties, J. Hazard. Mater. *455* (2023) 131649, https://doi.org/10.1016/j.jhazmat.2023.131649.

[30] Born, J.-P.; Van Brecht, A. Recycling potentials of MSWI Bottom Ash Available online: ⟨https://www.cewep.eu/wp-content/uploads/2017/10/1318_avb_and_jp_born_2014_cewep_conference_bottom_ash_reuse.pdf⟩ (accessed on Jan 27, 2022).

[31] M. Van Praagh, M. Johansson, J. Fagerqvist, R. Grönholm, N. Hansson, H. Svensson, Recycling of MSWI-bottom ash in paved constructions in Sweden – A risk assessment, Waste Manag *79* (2018) 428–434, https://doi.org/10.1016/j.wasman.2018.07.025.

[32] F. Becquart, F. Bernard, N. Edine, R. Zentar, Monotonic aspects of the mechanical behaviour of bottom ash from municipal solid waste incineration and its potential use for road construction, Waste Manag. *29* (2009) 1320–1329, https://doi.org/10.1016/j.wasman.2008.08.019.

[33] G. Gupta, M. Datta, G.V. Ramana, B.J. Alappat, MSW incineration bottom ash (MIBA) as a substitute to conventional materials in geotechnical applications: a characterization study from India and comparison with literature, Constr. Build. Mater. *308* (2021) 124925, https://doi.org/10.1016/j.conbuildmat.2021.124925.

[34] H.N. Le, A. Razakamanantsoa, M. Nguyen, V.T. Phan, P. Dao, D.H. Nguyen, Evaluation of physicochemical and hydromechanical properties of MSWI bottom ash for road construction, Waste Manag. *80* (2018) 168–174, https://doi.org/10.1016/j.wasman.2018.09.007.

[35] C.-L. Lin, M.-C. Weng, C.-H. Chang, Effect of incinerator bottom-ash composition on the mechanical behavior of backfill material, J. Environ. Manag. *113* (2012) 377–382, https://doi.org/10.1016/j.jenvman.2012.09.013.

[36] Y. Huang, J. Chen, S. Shi, B. Li, J. Mo, Q. Tang, Mechanical properties of municipal solid waste incinerator (MSWI) bottom ash as alternatives of subgrade materials, Adv. Civ. Eng. (2020) 1–11.

[37] R. Xie, Y. Xu, M. Huang, H. Zhu, F. Chu, Assessment of municipal solid waste incineration bottom ash as a potential road material, Road. Mater. Pavement Des. ISSN *18* (2017) 992–998, https://doi.org/10.1080/14680629.2016.1206483.

[38] B. Muhunthan, R. Taha, J. Said, Geotechnical engineering properties of incinerator ash mixes, J. Air Waste Manag. Assoc. *54* (2004) 985–991, https://doi.org/10.1080/10473289.2004.10470959.

[39] N.C. Lan, N.H. Ha, N.A. Tuan, V.A. Tuan, N.H. Dong, Static and cyclic properties of municipal solid bottom ash in VietnaM, Int. J. Geomate *20* (2021) 152–158.

[40] N.H. Le, N.E. Abriak, C. Binetruy, M. Benzerzour, S.T. Nguyen, Mechanical behavior of municipal solid waste incinerator bottom ash: results from triaxial tests, Waste Manag *65* (2017) 37–46, https://doi.org/10.1016/j.wasman.2017.03.045.

[41] E. Toraldo, S. Saponaro, A road pavement full-scale test track containing stabilized bottom ashes, Environ. Technol. *36* (2015) 1114–1122, https://doi.org/10.1080/09593330.2014.982714.

[42] European Commission Circular economy action plan Available online: ⟨https://environment.ec.europa.eu/strategy/circular-economy-action-plan_en⟩ (accessed on May 12, 2023).

[43] B.S. Bandarra, L.A. Gomes, J.L. Pereira, F.J.M. Gonçalves, R.C. Martins, M. J. Quina, Characterization of ecotoxicological effects of green liquor dregs from the pulp and paper industry, ACS Sustain. Chem. Eng. *7* (2019) 14707–14715, https://doi.org/10.1021/acssuschemeng.9b02636.

[44] B.S. Bandarra, L.A. Gomes, J.L. Pereira, F.J.M. Gonçalves, R.C. Martins, M. J. Quina, Assessment of hazardous property HP 14 using ecotoxicological tests: a case study of weathered coal fly ash, Environ. Sci. Pollut. Res. *27* (2020) 20972–20983, https://doi.org/10.1007/s11356-020-08515-8.

[45] 11348-2, I. Water quality — determination of the inhibitory effect of water samples on the light emission of Vibrio fischeri (luminescent bacteria test) — part 2: method using liquid-dried bacteria. International Organisation for Standardisation. Geneva. 2007.

[46] OECD Test No. 201: freshwater alga and cyanobacteria, growth inhibition test. OECD guidelines for the testing of chemicals, Section 2. OECD Editions. Paris. 2006.

[47] S.W. Geis, K.L. Fleming, E.T. Korthals, G. Searle, L. Reynolds, D.A. Karner, Modifications to the algal growth inhibition test for use as a regulatory assay, Environ. Toxicol. Chem. *19* (2000) 36–41, https://doi.org/10.1897/1551-5028(2000)019<0036:mttagi>2.3.co;2.

[48] OECD Test no. 221: Lemna sp. growth inhibition test. OECD guidelines for the testing of chemicals, Section 2. OECD editions. Paris. 2006.

[49] M. Kaza, J. Mankiewicz-Boczek, K. Izydorczyk, J. Sawicki, Toxicity assessment of water samples from rivers in central Poland using a battery of microbiotests - A pilot study. *Polish J. Environ*, Stud *16* (2007) 81–89.

[50] OECD Test no. 202: Daphnia sp. acute immobilisation test. OECD guidelines for the testing of chemicals, Section 2. OECD editions. Paris. 2004.

[51] 18763, I. Soil quality — Determination of the toxic effects of pollutants on germination and early growth of higher plants. International Organisation for Standardisation, Geneva. 2016.

[52] M.M. El-Deeb Ghazy, M.M. Habashy, E.Y. Mohammady, Effects of pH on survival, growth and reproduction rates of the crustacean, Daphnia Magna. *Aust. J. Basic Appl. Sci. 5* (2011) 1–10.

[53] R.R. Karna, T. Luxton, K.E. Bronstein, J. Hoponick Redmon, K.G. Scheckel, State of the science review: potential for beneficial use of waste by-products for in situ remediation of metal-contaminated soil and sediment, Crit. Rev. Environ. Sci. Technol. *47* (2017) 1–65, https://doi.org/10.1080/10643389.2016.1275417.

[54] R.A. Festa, D.J. Thiele, Copper: an essential metal in biology, Curr. Biol. *21* (2011) R877–R883, https://doi.org/10.1016/j.cub.2011.09.040.

[55] C.J. Lynn, G.S. Ghataora, R.K. Dhir OBE, Municipal incinerated bottom ash (MIBA) characteristics and potential for use in road pavements, Int. J. Pavement Res. Technol. *10* (2017) 185–201, https://doi.org/10.1016/j.ijprt.2016.12.003.

[56] T. Astrup, A. Muntoni, A. Polettini, R. Pomi, T. Van Gerven, A. Van Zomeren, Treatment and Reuse of Incineration Bottom Ash, in: M.N.V. Prasad, K. Shih (Eds.), In *Environmental Materials and Waste: Resource Recovery and Pollution Prevention.*, Elsevier, 2016, pp. 607–645.

[57] R.C.C. Monteiro, C.F. Figueiredo, M.S. Alendouro, M.C. Ferro, E.J.R. Davim, M.H. V. Fernandes, Characterization of MSWI bottom ashes towards utilization as glass raw material, Waste Manag. *28* (2008) 1119–1125, https://doi.org/10.1016/j.wasman.2007.05.004.

[58] F. Neuwahl, G. Cusano, J.G. Benavides, S. Holbrook, R. Serge, Best Available Techniques (BAT) Reference Document for Waste Incineration. Industrial Emissions Directive 2010/75/EU (Integrated Pollution Prevention). Science for Policy report by the Joint Research Centre, European Commission, Luxembourg, 2019.

[59] E. Rambaldi, L. Esposito, F. Andreola, L. Barbieri, I. Lancellotti, I. Vassura, The recycling of MSWI bottom ash in silicate based ceramic, Ceram. Int. *36* (2010) 2469–2476, https://doi.org/10.1016/j.ceramint.2010.08.005.

[60] E. Rendek, G. Ducom, P. Germain, Influence of waste input and combustion technology on MSWI bottom ash quality, Waste Manag. *27* (2007) 1403–1407, https://doi.org/10.1016/j.wasman.2007.03.016.

[61] P. Tang, M.V.A. Florea, P. Spiesz, H.J.H. Brouwers, Characteristics and application potential of municipal solid waste incineration (MSWI) bottom ashes from two waste-to-energy plants, Constr. Build. Mater. *83* (2015) 77–94, https://doi.org/10.1016/j.conbuildmat.2015.02.033.

[62] Z. Zhang, L. Zhang, A. Li, Development of a sintering process for recycling oil shale fly ash and municipal solid waste incineration bottom ash into glass ceramic composite, Waste Manag. *38* (2015) 185–193, https://doi.org/10.1016/j.wasman.2014.12.028.

[63] A.P. Bayuseno, W.W. Schmahl, Understanding the chemical and mineralogical properties of the inorganic portion of MSWI bottom ash, Waste Manag *30* (2010) 1509–1520, https://doi.org/10.1016/j.wasman.2010.03.010.

[64] J. Hyks, T. Astrup, T.H. Christensen, Leaching from MSWI bottom ash: evaluation of non-equilibrium in column percolation experiments, Waste Manag *29* (2009) 522–529, https://doi.org/10.1016/j.wasman.2008.06.011.

[65] D. Lindberg, C. Molin, M. Hupa, Thermal treatment of solid residues from WtE units: a review, Waste Manag *37* (2015) 82–94, https://doi.org/10.1016/j.wasman.2014.12.009.

[66] J. Tang, B.M. Steenari, Leaching optimization of municipal solid waste incineration ash for resource recovery: a case study of Cu, Zn, Pb and Cd, Waste Manag *48* (2016) 315–322, https://doi.org/10.1016/j.wasman.2015.10.003.

[67] N. Cristelo, L. Segadães, J. Coelho, B. Chaves, N.R. Sousa, M. de Lurdes Lopes, Recycling municipal solid waste incineration slag and fly ash as precursors in low-range alkaline cements, Waste Manag. *104* (2020) 60–73, https://doi.org/10.1016/j.wasman.2020.01.013.

[68] Klymko, T.; Dijkstra, J.J.; van Zomeren, A. *Guidance document on hazard classification of MSWI bottom ash. ECN report*; Petten, the Netherlands, 2017;

[69] A.J. Chandler, T.T. Eighmy, J. Hartlén, O. Hjelmar, D.S. Kosson, S.E. Sawell, H.A. van der Sloot, J. Vehlow, *Municipal Solid Waste Incinerator Residues. The International Ash Working Group (IAWG)*; Studies in Environmental Science, 67. Elsevier, Amsterdam, The Netherlands, 1997. ISBN 0444825630.

[70] Bunge, R. Recovery of Metals from Waste Incineration Bottom Ash. In *Treatment and Utilisation of Waste Incineration Bottom Ash*; Holm, O., Thome-Kozmiensky, E., Eds.; Neuruppin, Germany, 2018; pp. 63–143.

[71] F. Andreola, L. Barbieri, S. Hreglich, I. Lancellotti, L. Morselli, F. Passarini, I. Vassura, Reuse of incinerator bottom and fly ashes to obtain glassy materials, J. Hazard. Mater. *153* (2008) 1270–1274, https://doi.org/10.1016/j.jhazmat.2007.09.103.

[72] M.S. Ashraf, Z. Ghouleh, Y. Shao, Production of eco-cement exclusively from municipal solid waste incineration residues, Resour. Conserv. Recycl. *149* (2019) 332–342, https://doi.org/10.1016/j.resconrec.2019.06.018.

[73] R. Forteza, M. Far, C. Seguí, V. Cerdá, Characterization of bottom ash in municipal solid waste incinerators for its use in road base, Waste Manag. *24* (2004) 899–909, https://doi.org/10.1016/j.wasman.2004.07.004.

[74] O. Ginés, J.M. Chimenos, A. Vizcarro, J. Formosa, J.R. Rosell, Combined use of MSWI bottom ash and fly ash as aggregate in concrete formulation: Environmental and mechanical considerations, J. Hazard. Mater. *169* (2009) 643–650, https://doi.org/10.1016/j.jhazmat.2009.03.141.

[75] F. Huber, D. Blasenbauer, P. Aschenbrenner, J. Fellner, Chemical composition and leachability of differently sized material fractions of municipal solid waste incineration bottom ash, Waste Manag. *95* (2019) 593–603, https://doi.org/10.1016/j.wasman.2019.06.047.

[76] Maria, I.; Enric, V.; Xavier, Q.; Barra, M.; López, A.; Plana, F. Use of bottom ash from municipal solid waste incineration as a road material. In Proceedings of the International Ash Utilization Symposium, Center for Applied Energy Research, University of Kentucky; 2001.

[77] B. Gao, Phosphorus Recovery from Sorted MSWI Bottom Ash: the acidic dissolution – precipitation method, Chalmers University of Technology, Göteborg, Sweden, 2012.

[78] S. Sorlini, M.C. Collivignarelli, A. Abbà, Leaching behaviour of municipal solid waste incineration bottom ash: from granular material to monolithic concrete, Waste Manag. Res. *35* (2017) 978–990, https://doi.org/10.1177/0734242×17721340.

[79] J.M. Chimenos, A.I. Fernández, L. Miralles, M. Segarra, F. Espiell, Short-term natural weathering of MSWI bottom ash as a function of particle size, Waste Manag *23* (2003) 887–895, https://doi.org/10.1016/S0956-053X(03)00074-6.

[80] LNEC - Laboratório Nacional de Engenharia Civil. *Documento de aplicação. AEIRU - Agregados artificiais de escórias de incineração de resíduos urbanos para pavimentos rodoviários*; Lisbon, Portugal, 2015;

[81] B.S. Bandarra, J.L. Pereira, R.C. Martins, A. Maldonado-Alameda, J.M. Chimenos, M.J. Quina, Opportunities and barriers for valorizing waste incineration bottom ash: Iberian countries as a case study, Appl. Sci. *11* (2021) 9690, https://doi.org/10.3390/app11209690.

[82] M. Di Gianfilippo, J. Hyks, I. Verginelli, G. Costa, O. Hjelmar, F. Lombardi, Leaching behaviour of incineration bottom ash in a reuse scenario: 12 years-field data vs. lab test results, Waste Manag. *73* (2018) 367–380, https://doi.org/10.1016/j.wasman.2017.08.013.

[83] Fulladosa, E.; Murat, J.C.; Martínez, M.; Villaescusa, I. Patterns of metals and arsenic poisoning in Vibrio fischeri bacteria. 2005, *60*, 43–48, ⟨doi:10.1016/j.chemosphere.2004.12.026⟩.

[84] S. Stiernström, K. Hemström, O. Wik, G. Carlsson, B.E. Bengtsson, M. Breitholtz, An ecotoxicological approach for hazard identification of energy ash, Waste Manag. *31* (2011) 342–352, https://doi.org/10.1016/j.wasman.2010.05.019.

[85] H. Moser, J. Roembke, G. Donnevert, R. Becker, Ecotoxicological Character Waste.: Results Exp. a Eur. Ring Test. (2009) *11*.

[86] M. Bożym, A. Król, K. Mizserna, Leachate and contact test with Lepidium sativum L. to assess the phytotoxicity of waste, Int. J. Environ. Sci. Technol. *18* (2021) 1975–1990, https://doi.org/10.1007/s13762-020-02980-x.

[87] J. Tintner, L. Matiasch, B. Klug, Germination and juvenile development of plants on municipal solid waste incineration (MSWI) slag, Ecol. Eng. *87* (2016) 162–167, https://doi.org/10.1016/j.ecoleng.2015.11.037.

[88] A. Sridharan, Y. Gurtug, Swelling behaviour of compacted fine-grained soils, Eng. Geol. *72* (2004) 9–18, https://doi.org/10.1016/S0013-7952(03)00161-3.

[89] E. Loginova, D.S. Volkov, P.M.F.Van De Wouw, M.V.A. Florea, H.J.H. Brouwers, Detailed characterization of particle size fractions of municipal solid waste incineration bottom ash, J. Clean. Prod. *207* (2020) 866–874, https://doi.org/10.1016/j.jclepro.2018.10.022.

[90] J. Ameratunga, N. Sivakugan, B.M. Das, Correlations of soil and rock properties in geotechnical engineering, Springer, New Delhi, 2016.

[91] S.A.N.M. Yusoff, I. Bakar, D.C. Wijeyesekera, A. Zainorabidin, M. Azmi, H. Ramli, The effects of different compaction energy on geotechnical properties of kaolin and laterite, AIP Conf. Proc. (2017) *1875*, https://doi.org/10.1063/1.4998380.

[92] R.V. Silva, J. de Brito, C.J. Lynn, R.K. Dhir, Use of municipal solid waste incineration bottom ashes in alkali-activated materials, ceramics and granular applications: a review, Waste Manag *68* (2017) 207–220, https://doi.org/10.1016/j.wasman.2017.06.043.

[93] M. Zamani, K. Badv, Assessment of the geotechnical behavior of collapsible soils: a case study of the Mohammad-abad railway station soil in semnan, Geotech. Geol. Eng. *37* (2019) 2847–2860, https://doi.org/10.1007/s10706-018-00800-1.

[94] Y. Lins, T. Schanz, Determination of hydro-mechanical Properties of Sand, in: T. Schanz (Ed.), Unsaturated soils: experimental studies, Springer, Berlim, Germany, 2003, pp. 15–32.

[95] P.N., P. Raju, N.S. Andian, T.S. Nagaraj, Analysis and estimation of the coefficient of consolidation, Geotech. Test. J. ASTM *18* (1995) 252–258.

[96] B.M. Das. Advanced Soil Mechanics, 5th Editio, CRC Press, Boca Raton, Florida, 2019 (Taylor & Francis Group).

[97] G. Mesri, B. Vardhanabhuti, Compression of granular materials, Can. Geotech. J. (2009) 369–392.

[98] J. Zheng, R.D. Hryciw, A. Ventola, Compressibility of sands of various geologic origins at pre-crushing stress levels, Geotech. Geol. Eng. *35* (2017) 2037–2051, https://doi.org/10.1007/s10706-017-0225-9.

[99] R.F. Craig. Craig's Soil Mechanics, 7th ed., Spon Press, 2004 (Taylor & Francis Group: London and New York).

[100] N.R. Regmi, J.R. Giardino, E.V. McDonald, J.D. Vitek, A review of mass movement processes and risk in the critical zone of Earth, Dev. Earth Surf. Process. *19* (2015) 319–362.

[101] N. Sivakugan, Engineering Properties of Soil, in: B.M. Das (Ed.), Geotechnical Engineering Handbook, J. Ross Publishing, Florida, 2011. ISBN 9781932159837.

[102] Ridley, A.M. Soil suction — what it is and how to successfully measure it. In Proceedings of the PFMGM 2015: Proceedings of the Ninth Symposium on Field Measurements in Geomechanics; Dight, P., Ed.; Australian Centre for Geomechanics: Perth, 2015; pp. 27–46.

[103] R.J. Azeiteiro, P.A. Coelho, D.M. Taborda, J.C. Grazina, Critical state–based interpretation of the monotonic behavior of Hostun sand, J. Geotech. Geoenviron. Eng. *143* (2017) 04017004.

[104] T. Godlewski, Evaluation of stiffness degradation curves from in situ tests in various soil types, Arch. Civ. Eng. *64* (2018) 285–307.